



Letters

A Phase-Shifted Square Wave Modulation (PS-SWM) for Modular Multilevel Converter (MMC) and DC Transformer for Medium Voltage Applications

Ran Mo , Member, IEEE, Hui Li , Fellow, IEEE, and Yanjun Shi, Senior Member, IEEE

Abstract—In this letter, a phase-shifted square wave modulation strategy is proposed for modular multilevel converters (MMCs) as well as dc transformers for medium-voltage applications. The proposed technique can achieve a smaller cell capacitor size without increasing the total device rating (TDR) and degrading the dc current control capability. The operation principle of the proposed method is presented on an isolated modular multilevel dc–dc converter, which consists of an MMC stage and applied as a dc transformer for medium-voltage dc grid. The TDR and passive components sizing are derived and compared with those using other modulation methods. Finally a downscaled hardware prototype has been built and tested to verify the proposed modulation method.

Index Terms—Cell capacitor, dc transformer, modular multilevel converter (MMC), MVDC, phase-shifted (PS) modulation.

I. INTRODUCTION

THE modular multilevel converter (MMC) has been applied to high/medium voltage direct current (HVDC/MVDC) grids [1], [2], medium voltage (MV) motor drive [3], [4], and dc transformers for an MVDC system [5], [6]. A phase-shifted sinusoidal modulation method is usually adopted for MMC. The MMC has many advantages including superior current control capability and no dc link capacitors; however, one demerit of MMC is the large cell capacitor size and high total device rating (TDR). Wang *et al.* has proposed a method to reduce the cell capacitor of MMC by applying a small arm inductance to achieve a capacitor charge balance in a switching cycle; however, this method may require a dc link capacitor to decouple the grid impedance effect to maintain a small arm inductance [7]. Another method can reduce the MMC cell capacitor size by injecting a second-harmonic component but leads to an increased TDR since circulation current becomes larger [8]. In addition, the methods proposed to reduce the MMC cell capacitors may not be the best choice for a dc transformer consisting of an MMC stage since a higher ac frequency and more modulation freedoms exist in a dc transformer.

In this letter, a phase-shifted square wave modulation (PS-SWM) method has been proposed to reduce the cell capacitor size and the TDR of an MMC. In addition, this method can achieve a small arm inductance but without requiring a dc link capacitor to decouple the grid impedance effect. This method has been applied to an isolated modular multilevel dc–dc converter (iM2DC) for an MVDC system application, which consists of an MMC stage and a medium frequency (MF) ac transformer. Various modulation methodologies have been proposed for the MV iM2DC including phase-shifted sinusoidal modulation [9]–[11], two-level (2L) and a quasi-two-level (Q2L) modulation [12]–[14], as well as triangular modulation [15]. Among these modulation methods, large cell capacitors are needed for sinusoidal modulation; triangular modulation, on the other hand, results in a large arm root mean square current leading to a higher TDR and conduction loss; a 2L and Q2L modulation can achieve smaller capacitors and TDR but at the cost of dc current control capability. With proposed PS-SWM, the MV iM2DC can achieve low passive component size without increasing TDR and degrading dc current control capability.

The letter is organized in the following way. In Section II, an iM2DC applied for the MVDC system is first introduced. The operation principle of the proposed PS-SWM modulation is, then, presented on the MMC stage of this MV iM2DC. The TDR and the sizing of cell capacitors as well as arm inductance are also derived in Section II and compared with those using PS sinusoidal and Q2L modulation methods. A downscaled hardware prototype has been built in the laboratory. The experimental waveforms of an MMC stage and an iM2DC are provided in Section III to verify the validity of the proposed modulation method. Finally, the proposed PS-SWM is summarized in Section IV.

II. OPERATION PRINCIPLES OF PS-SWM

The topology of an iM2DC applied as a dc transformer for an MVDC system is shown in Fig. 1. It consists of two sides integrating through an MF transformer. One side is connected to an MVDC bus. Multiple full-bridge cells or half-bridge cells are cascaded within each arm. Distributed cell capacitors are installed at the dc link of each cell and coupled arm inductors are adopted to achieve decoupled dc and ac inductance. Based on the application requirement, the other side can be connected

Manuscript received October 22, 2018; accepted November 21, 2018. Date of publication December 6, 2018; date of current version May 2, 2019. (Corresponding author: Hui Li.)

The authors are with the Center for Advanced Power Systems, Florida State University, Tallahassee, FL 32310 USA (e-mail: rmo@caps.fsu.edu; hli@caps.fsu.edu; yshi3@caps.fsu.edu).

Color versions of one or more of the figures in this letter are available online at <http://ieeexplore.ieee.org>.

Digital Object Identifier 10.1109/TPEL.2018.2885278

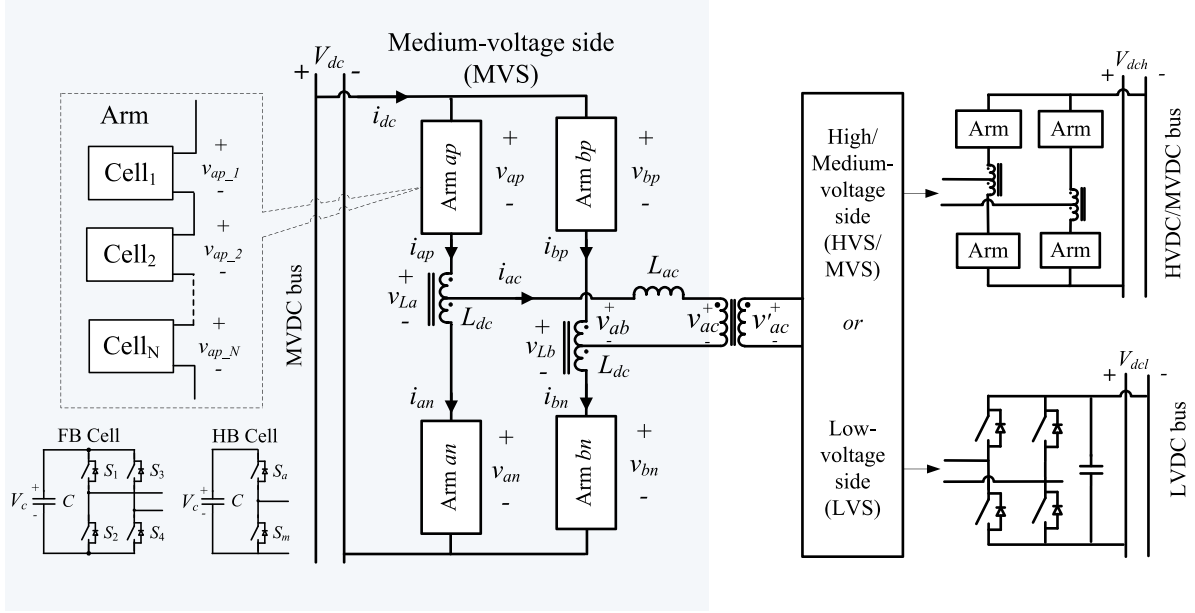


Fig. 1. Topology of an iM2DC consisting of an MMC stage at MVS connected to an MVDC bus.

to either an HVDC/MVDC bus with similar MMC structure, or a low-voltage dc bus with a 2L converter. The operation principle of the proposed PS-SWM will be illustrated on the MMC stage of the medium-voltage side (MVS), which is shown in Fig. 1.

The modulation waveforms of the proposed PS-SWM strategy as well as the corresponding arm voltages and transformer voltage are shown in Fig. 2. As shown in Fig. 2(a), a square waveform with 0.5 duty cycle is adopted as the modulation waveform, where magnitude M and dc offset d are controllable. $m_{a(b)p}$ and $m_{a(b)n}$ are the modulation waveforms of phase a (b) upper arm and lower arm, respectively. m_{ap} is the same as m_{bn} , which is 180° phase-shifted with the m_{an} and m_{bp} . N is the cell number in one arm, $C_1 \sim C_N$ are carrier waveforms with the frequency, which can be as low as twice of the modulation frequency. A phase-shifted angle $2\pi/N$ is applied among carriers, which increases the equivalent switching frequency. Consequently, the square arm voltage and transformer voltage waveforms will be formed with small high-frequency waveforms as shown in the zoomed-in view in Fig. 2(b). A large modulation index, i.e., a large M is desired, since v_{ab} can be as high as dc bus voltage V_{dc} , which achieves lowest converter TDR. In addition, the highest voltage ripple frequency and lowest ripple magnitude occur at the same time on the arm inductor voltage v_{La} and v_{Lb} in this mode, which indicates the smallest inductor size can be achieved.

A staircase or trapezoidal modulation waveform instead of a square wave can be utilized to reduce the ac voltage dv/dt . When the staircase level increases, v_{ab} has more levels and smaller dv/dt . Fig. 3 depicts the key waveforms of an iM2DC with the proposed modulation method. A 6L staircase wave modulation is applied, which already attains the same ac voltage level with that of the trapezoidal wave modulation and adequate for a reduced dv/dt performance. The operation principle of a secondary side is similar to that of the primary side, but with a phase shift angle φ to transfer the power. Although the magnitude of modulation waveform can vary in the secondary side

as well, usually it equals to that of the primary side modulation waveform to ensure high efficiency. Both dc bus current i_{dc} and transformer current i_{ac} flow through the cells, therefore, the arm current contains both dc and ac components as shown in Fig. 3 using the primary side phase a arm current i_{ap} and i_{an} as examples. Moreover, the small stair step angle α with acceptable dv/dt are preferred, otherwise the dc voltage utilization will be sacrificed. In this letter, this angle is assumed to be very small, such that they can be neglected in the following steady state analysis.

The TDR and the passive component size of proposed modulation method can be derived as follows. The arm voltage and arm current of an MMC stage in Fig. 1 can be written as

$$\begin{cases} v_{ap} = v_{bn} = \frac{V_{dc}}{2} - \frac{v_{ab}}{2}, v_{bp} = v_{an} = \frac{V_{dc}}{2} + \frac{v_{ab}}{2} \\ i_{ap} = i_{bn} = \frac{i_{dc}}{2} + \frac{i_{ab}}{2}, i_{bp} = i_{an} = \frac{i_{dc}}{2} - \frac{i_{ab}}{2}. \end{cases} \quad (1)$$

If ignoring the stair step angle and the high-frequency ripples, the ac voltage of an MMC stage can be considered as a pure square wave as

$$v_{ab} = V_{ab} \cdot S[\theta], \quad S[\theta] = \begin{cases} 1, \theta \in [0, \pi] \\ -1, \theta \in [\pi, 2\pi] \end{cases} \quad (2)$$

where the magnitude of the ac voltage, V_{ab} , is adjustable with the proposed PS-SWM, which can be defined as

$$V_{ab} = k \cdot V_{dc} \quad (3)$$

where k is the voltage ratio of ac-to-dc. The voltage and current stress of each device on an MMC stage is

$$v_s = \frac{V_{dc}}{2N} + \frac{V_{ab}}{N}, \quad i_s = \frac{i_{dc}}{2} + \frac{i_{ac}}{2}. \quad (4)$$

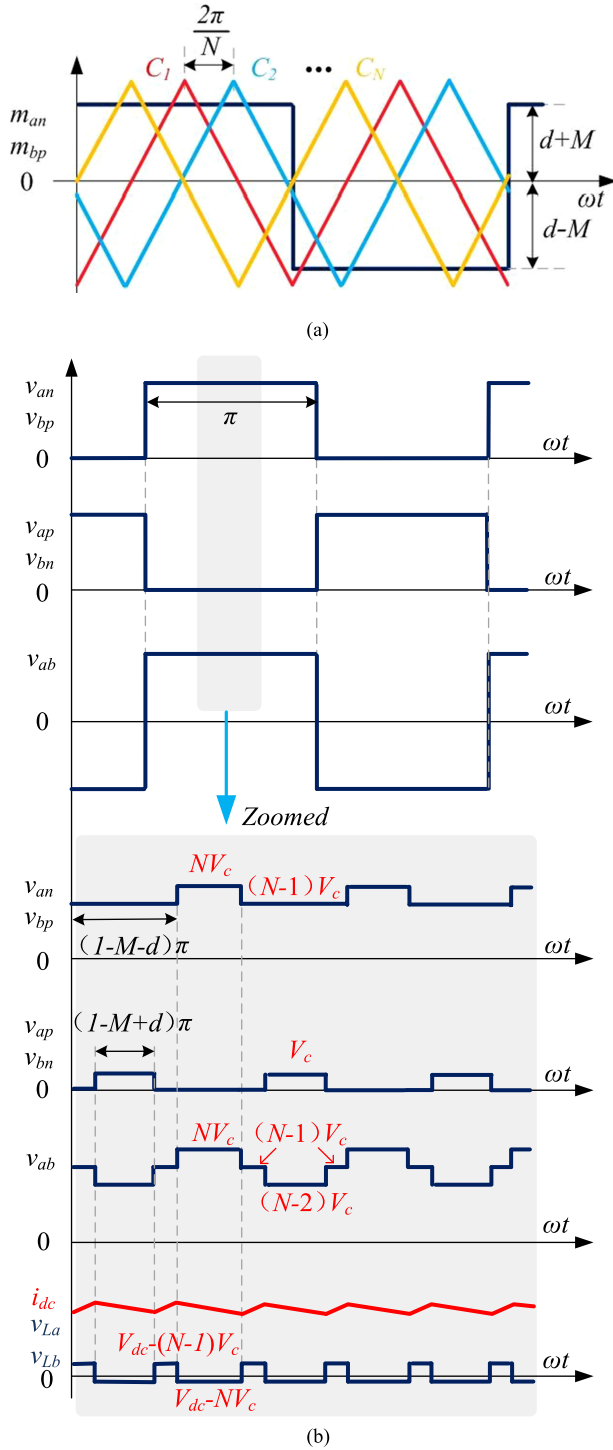


Fig. 2. PS-SWM modulation and key waveforms of an MMC stage in an iM2DC. (a) Modulation waveform. (b) Zoomed key waveforms.

Then, the TDR of an iM2DC MVS MMC stage can be derived in (5), where P is the power rating of converter

$$\begin{aligned} \text{TDR}_{\text{MVS}} &= 4N \cdot \left(\frac{V_{\text{dc}}}{2N} + \frac{v_{ab}}{2N} \right) \cdot \sqrt{\left(\frac{i_{\text{dc}}}{2} \right)^2 + \left(\frac{i_{\text{sc}}}{2} \right)^2} \\ &= P \cdot (1+k) \cdot \sqrt{1 + \frac{1}{k^2}}. \end{aligned} \quad (5)$$

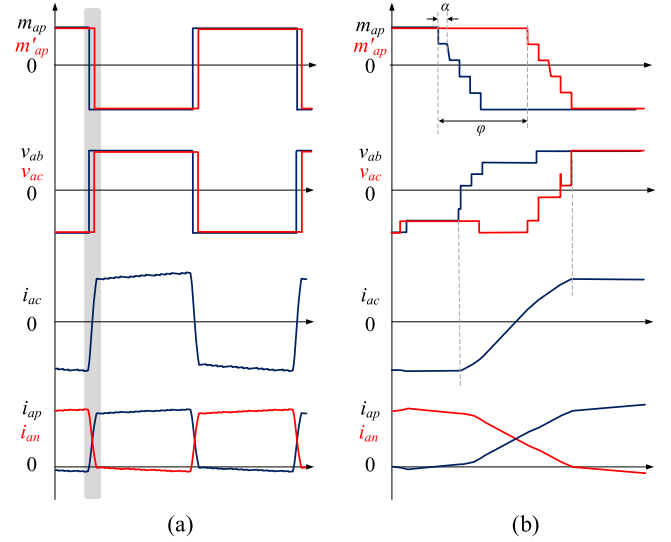


Fig. 3. Key waveforms of an iM2DC consisting of two MMC stages applying PS-SWM modulation. (a) Transformer voltage, current, and arm current. (b) Zoomed view of the shaded range in (a).

Based on (5), the minimal TDR can be accomplished when $k = 1$, i.e., the ac voltage magnitude equals to dc bus voltage.

The cell capacitors in an MMC with the proposed PS-SWM can be much smaller since they can be designed to smooth the high switching frequency ripples only because of a square wave at an ac terminal. With $k = 1$, the size of cell capacitor with the proposed modulation is derived in (6) by applying a capacitor charge-balance in a switching cycle as

$$\begin{aligned} C &= \left(\frac{I_{\text{dc}}}{2} + \frac{I_{\text{ac}}}{2} \right) \cdot \frac{1}{\sigma \cdot V_C} \left[\frac{\pi(d-M+1)}{\omega} + \frac{|\varphi|}{2\omega_{\text{tr}}} \right] \\ &\approx \frac{I_{\text{dc}}}{\sigma \cdot V_C} \left[\frac{\pi|d|}{\omega} + \frac{|\varphi|}{2\omega_{\text{tr}}} \right] \end{aligned} \quad (6)$$

where ω and ω_{tr} are the angular cell switching frequency and transformer frequency, respectively, I_{dc} is the nominal dc current, σ is the peak-peak capacitor voltage ripple percentage. Since $M \approx 1$ is desired in the application, the capacitance can be simplified as shown in (6).

The arm inductance of an iM2DC in Fig. 1, L_{dc} , is also small considering the equivalent dc current ripple frequency is $2 \cdot N$ times of the cell switching frequency with the proposed modulation. L_{dc} can be calculated in (7), where γ is the peak-peak dc current ripple percentage. Since d is usually very small, the inductance can be simplified as

$$\begin{aligned} L_{\text{dc}} &= \frac{2\pi \cdot V_{\text{dc}}}{\omega \cdot \gamma \cdot I_{\text{dc}}} \cdot |d| \cdot \left(1 - \frac{N-1}{(1+d)N} \right) \\ &\approx \frac{2\pi \cdot V_{\text{dc}}}{\omega \cdot N \cdot \gamma \cdot I_{\text{dc}}} \cdot |d|. \end{aligned} \quad (7)$$

The TDR and passive components of the iM2DC consisting two symmetrical MMC stages can be derived similarly and compared with those using a Q2L [13] and PS sinusoidal modulation method in Table I. The TDR of PS-SWM and Q2L is 18% less than that of PS sinusoidal modulation due to the higher efficient

TABLE I
COMPARISON OF AN IM2DC WITH DIFFERENT MODULATION METHODS

Modulation method	TDR/P (p.u.)	Total cell capacitor energy (p.u.) $\frac{J}{KVA} \cdot S^{-1}$	L_{dc}
PS sinusoidal	$4\sqrt{3}$	$\frac{3\sqrt{3}}{4\pi\sigma}$	$\frac{\pi \cdot V_C}{N \cdot \omega \cdot \gamma \cdot I_{dc}}$
Q2L [13]	$4\sqrt{2}$	$\frac{ \phi }{\pi\sigma} + \frac{2(1-2D)}{\sigma}$	$\frac{2\pi \cdot V_{dc} \cdot (1-2D)}{\omega \cdot \gamma \cdot I_{dc}}$
Proposed PS-SWM	$4\sqrt{2}$	$\frac{ \phi }{\pi\sigma} + \frac{2 d }{\sigma} \cdot \frac{f_{tr}}{f}$	$\frac{2\pi \cdot V_{dc} \cdot d }{N \cdot \omega \cdot \gamma \cdot I_{dc}}$

power transfer capability of square wave. The per unit of total capacitor energy, defined as total capacitor energy \times fundamental frequency / rated power is adopted to evaluate the capacitor size in Table I, where f_{tr} and f are the transformer frequency and cell switching frequency, respectively. With PS sinusoidal modulation, the cell capacitors have to withstand both the fundamental and double frequency energy variations [16]. Although the fundamental frequency voltage ripple can be eliminated by some methods to achieve smaller capacitors, those methods will result in higher TDR. On the other hand, the cell capacitor with Q2L [13] and the proposed PS-SWM can be much smaller since only higher switching frequency ripple exists when $k = 1$. Considering the voltage ripple, current ripple, and thermal stress, the cell capacitors using a Q2L and PS-SWM will have similar size. Table I also compares the coupled arm inductors (L_{dc}) using a Q2L [13] and PS-SWM when $k = 1$, which are both designed to limit the dc current switching ripple. Since $1-2D$ of the Q2L (D is duty cycle) and $|d|$ of the proposed PS-SWM will have similar values under same converter ratings, L_{dc} with PS-SWM will be approximately N times smaller than that with Q2L. The L_{dc} of PS sinusoidal modulation will be similar to that of PS-SWM due to the voltage applied on L_{dc} is one cell voltage in the former modulation and the inductor voltage is the difference between dc grid voltage and the total capacitor voltage of a leg in the latter modulation method. In addition, the equivalent dc current ripple frequency of both modulation methods is $2 \cdot N$ times of the cell switching frequency because of a phase-shifted carrier wave nature.

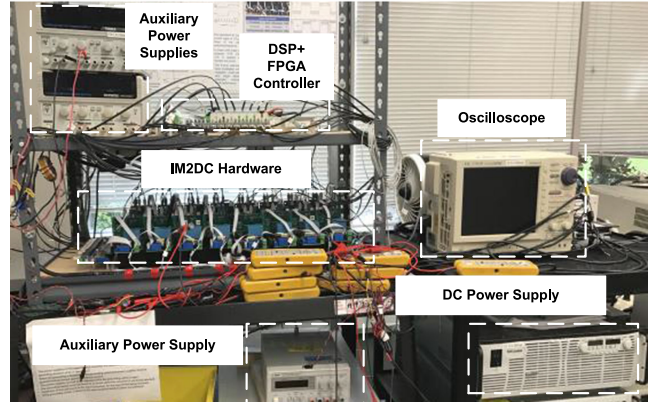
III. EXPERIMENTAL VERIFICATION

A downscaled prototype has been built in the laboratory to verify the proposed modulation method. The hardware is shown in Fig. 4 with the circuit parameters presented in Table II. The hardware can be configured as a single MMC stage or a dc transformer consisting of two MMC stages connected back-to-back through a 40-kHz ac transformer. The experiments were first conducted on a single MMC stage connected to an resistor-inductor load with four cells in each arm to demonstrate the proposed PS-SWM modulation. The fundamental frequency or transformer frequency is selected as 10 kHz and the switching frequency is designed at 40 kHz to ensure the quality of ac terminal voltage since this downscaled hardware has a limited cell number on each arm.

When the hardware is configured as a single MMC stage, the converter is operated at 2 kW power rating and 250 V dc



(a)



(b)

Fig. 4. Experimental setup. (a) Downscaled hardware prototype. (b) Testbed.

TABLE II
CIRCUIT PARAMETERS OF THE DOWNSCALED HARDWARE

Arm inductor L_{dc} : 100 μ H	AC inductor L_{ac} : 25 μ H
Switching frequency f : 40kHz	transformer frequency f_{tr} : 10kHz
Cell MOSFETs: IRFP260N	Cell capacitor C : 20 μ F

input voltage. Fig. 5(a) demonstrates the key waveforms of a single MMC stage. The arm voltages $v_{a(b)p(n)}$ and ac terminal voltage v_{ab} exhibits the square wave with equivalent switching frequency ripples at 160 kHz in the given experimental condition. Fig. 5(b) shows the key waveforms at 1 kW/150 V operating conditions when this hardware is configured as an iM2DC consisting two MMC stages with a 1:1 transformer at 10 kHz. In this operation condition, each arm has two cells and the maximum power is 1 kW. A fixed phase-shift angle is applied between the modulation waveforms of two sides. It shows that the power can be transferred to the other side and the secondary dc bus voltage can be established. The cell capacitor voltages are stabilized as well.

The ac terminal voltage v_{ab} of Fig. 5(a) and (b) is consistent with theoretical analysis of Fig. 2(b). When cell number N is 2, three voltage steps of v_{ab} (NV_C , $(N-1)V_C$, $(N-2)V_C$) are $2V_C$, V_C , and 0, respectively; when cell number is 4, three voltage steps of v_{ab} are $4V_C$, $3V_C$, and $2V_C$, respectively. When cell

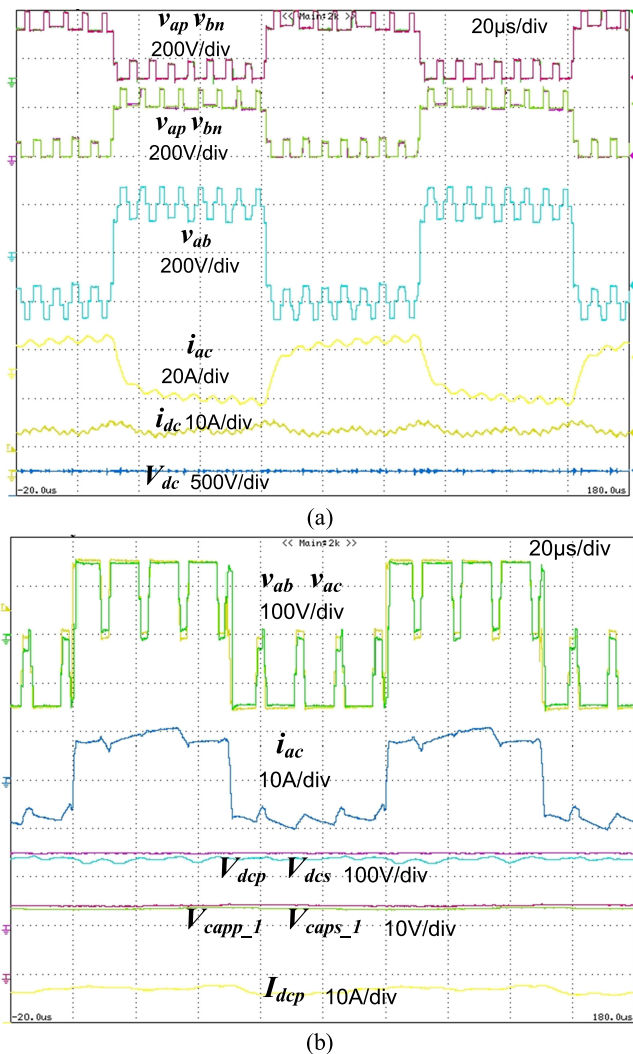


Fig. 5. Experimental results. (a) Key waveforms of a single MMC stage at 2 kW/250 V dc. (b) Key waveforms of an iM2DC at 1 kW/150 V dc.

number continues to increase, these voltage steps will become smaller compared to the voltage magnitude NV_C , therefore, v_{ab} will be close to a square wave for MV applications with a large number of cell numbers in each arm. The transformer current i_{ac} of Fig. 5(b) should be a square wave but demonstrates some distortions due to the open loop control leading to a not well balanced capacitor voltage, which can be solved by a closed-loop control.

IV. CONCLUSION

In this letter, a PS-SWM technique has been proposed. This modulation method can be applied for an MMC to reduce the cell capacitor size without a TDR penalty. In addition, an isolated dc–dc converter applied as a dc transformer for an MVDC system can also benefit from the proposed modulation method to achieve superior current control capability with a low passive component size while in the past an MV iM2DC cannot achieve both low passive component size and superior current control

capability at the same time. The detailed operation principles are presented and the sizing of passive components are derived. The comparison shows the proposed modulation method can achieve overall low TDR and low passive components.

REFERENCES

- [1] S. Debnath, J. Qin, B. Bahrani, M. Saeedifard, and P. Barbosa, "Operation, control, and applications of the modular multilevel converter: A review," *IEEE Trans. Power Electron.*, vol. 30, no. 1, pp. 37–53, Jan. 2015.
- [2] A. Nami, J. Liang, F. Dijkhuizen, and G. D. Demetriades, "Modular multilevel converters for HVDC applications: Review on converter cells and functionalities," *IEEE Trans. Power Electron.*, vol. 30, no. 1, pp. 18–36, Jan. 2015.
- [3] Y. Okazaki *et al.*, "Experimental comparisons between modular multilevel DSCC inverters and TSBC converters for medium-voltage motor drives," *IEEE Trans. Power Electron.*, vol. 32, no. 3, pp. 1805–1817, Mar. 2017.
- [4] L. He, K. Zhang, J. Xiong, S. Fan, and Y. Xue, "Low-frequency ripple suppression for medium-voltage drives using modular multilevel converter with full-bridge submodules," *IEEE J. Emerg. Sel. Topics Power Electron.*, vol. 4, no. 2, pp. 657–667, Jun. 2016.
- [5] S. Cui, N. Soltan, and R. W. de Doncker, "A high step-up ratio soft-switching DC–DC converter for interconnection of MVDC and HVDC grids," *IEEE Trans. Power Electron.*, vol. 33, no. 4, pp. 2986–3001, Apr. 2018.
- [6] Y. Chen, S. Zhao, Z. Li, X. Wei, and Y. Kang, "Modeling and control of the isolated DC–DC modular multilevel converter for electric ship medium voltage direct current power system," *IEEE J. Emerg. Sel. Topics Power Electron.*, vol. 5, no. 1, pp. 124–139, Mar. 2017.
- [7] J. Wang, R. Burgos, and D. Boroyevich, "Switching-cycle state-space modeling and control of the modular multilevel converter," *IEEE J. Emerg. Sel. Topics Power Electron.*, vol. 2, no. 4, pp. 1159–1170, Dec. 2014.
- [8] J. Pou, S. Ceballos, G. Konstantinou, V. G. Agelidis, R. Picas, and J. Zaragoza, "Circulating current injection methods based on instantaneous information for the modular multilevel converter," *IEEE Trans. Ind. Electron.*, vol. 62, no. 2, pp. 777–788, Feb. 2015.
- [9] T. L'uth, M. M. C. Merlin, T. C. Green, F. Hassan, and C. D. Barker, "High-frequency operation of a dc/ac/dc system for HVDC applications," *IEEE Trans. Power Electron.*, vol. 29, no. 8, pp. 4107–4115, Aug. 2014.
- [10] F. Sasongko, M. Hagiwara, and H. Akagi, "A front-to-front (FTF) system consisting of multiple modular multilevel cascade converters for offshore wind farms," in *Proc. Int. Conf. IEEE Power Electron.*, 2014, pp. 1761–1768.
- [11] Y. Chen, S. Zhao, Z. Li, X. Wei, and Y. Kang, "Modeling and control of the isolated DC–DC modular multilevel converter for electric ship medium voltage direct current power system," *IEEE J. Emerg. Sel. Topics Power Electron.*, vol. 5, no. 1, pp. 124–139, Mar. 2017.
- [12] I. Gowaid, G. Adam, A. Massoud, S. Ahmed, D. Holliday, and B. Williams, "Quasi two-level operation of modular multilevel converter for use in a high-power DC transformer with DC fault isolation capability," *IEEE Trans. Power Electron.*, no. 1, vol. 30, pp. 108–123, Jan. 2015.
- [13] Y. Shi and H. Li, "Isolated modular multilevel DC–DC converter with DC fault current control capability based on current-fed dual active bridge for MVDC application," *IEEE Trans. Power Electron.*, vol. 33, no. 3, pp. 2145–2161, Mar. 2018.
- [14] S. Kenzelmann, A. Rufer, D. Dujic, F. Canales, and Y. R. De Novaes, "Isolated DC/DC structure based on modular multilevel converter," *IEEE Trans. Power Electron.*, vol. 30, no. 1, pp. 89–98, Jan. 2015.
- [15] B. Zhao, Q. Song, J. Li, Y. Wang, and W. Liu, "Modular multilevel high-frequency-link dc transformer based on dual active phase-shift principle for medium-voltage dc power distribution application," *IEEE Trans. Power Electron.*, vol. 32, no. 3, pp. 1779–1791, Mar. 2017.
- [16] K. Ilves, S. Norrga, L. Harnefors, and H. -P. Nee, "On energy storage requirements in modular multilevel converters," *IEEE Trans. Power Electron.*, vol. 29, no. 1, pp. 77–88, Jan. 2014.